Ocean Sci., 11, 743–757, 2015
www.ocean-sci.net/11/743/2015/
doi:10.5194/os-11-743-2015

Ocean Science
Open Access

Transport of volume, heat, and salt towards the Arctic in the Faroe Current 1993–2013

B. Hansen[1], K. M. H. Larsen[1], H. Hátún[1], R. Kristiansen[1], E. Mortensen[1], and S. Østerhus[2]

[1]Faroe Marine Research Institute, Tórshavn, Faroe Islands
[2]Uni Research Climate, Bergen, Norway

Correspondence to: B. Hansen (bogihan@hav.fo)

Received: 24 April 2015 – Published in Ocean Sci. Discuss.: 9 June 2015
Revised: 29 August 2015 – Accepted: 8 September 2015 – Published: 22 September 2015

Abstract. The flow of warm and saline water from the Atlantic Ocean, across the Greenland–Scotland Ridge, into the Nordic Seas – the Atlantic inflow – is split into three separate branches. The most intense of these branches is the inflow between Iceland and the Faroe Islands (Faroes), which is focused into the Faroe Current, north of the Faroes. The Atlantic inflow is an integral part of the North Atlantic thermohaline circulation (THC), which is projected to weaken during the 21st century and might conceivably reduce the oceanic heat and salt transports towards the Arctic. Since the mid-1990s, hydrographic properties and current velocities of the Faroe Current have been monitored along a section extending north from the Faroe shelf. From these in situ observations, time series of volume, heat, and salt transport have previously been reported, but the high variability of the transport has made it difficult to establish whether there are trends. Here, we present results from a new analysis of the Faroe Current where the in situ observations have been combined with satellite altimetry. For the period 1993 to 2013, we find the average volume transport of Atlantic water in the Faroe Current to be 3.8 ± 0.5 Sv ($1\,\mathrm{Sv} = 10^6\,\mathrm{m^3\,s^{-1}}$) with a heat transport relative to 0 °C of 124 ± 15 TW ($1\,\mathrm{TW} = 10^{12}$ W). Consistent with other results for the Northeast Atlantic component of the THC, we find no indication of weakening. The transports of the Faroe Current, on the contrary, increased. The overall increase over the 2 decades of observation was 9 ± 8 % for volume transport and 18 ± 9 % for heat transport (95 % confidence intervals). During the same period, the salt transport relative to the salinity of the deep Faroe Bank Channel overflow (34.93) more than doubled, potentially strengthening the feedback on thermohaline intensity. The increased heat and salt transports are partly caused by the increased volume transport and partly by increased temperatures and salinities of the Atlantic inflow, which have been claimed mainly to be caused by the weakened subpolar gyre.

1 Introduction

The flow of warm and saline water from the Atlantic Ocean, across the Greenland–Scotland Ridge, into the Nordic Seas, the *Atlantic inflow*, occurs in three separate branches (plus flow over continental shelf areas). The two main branches pass between Iceland and the Scottish shelf on either side of the Faroes (Faroe Islands). This study treats the branch that flows between Iceland and the Faroes, the *IF inflow* (Fig. 1a), across the Iceland-Faroe Ridge (IFR) and continues in the *Faroe Current*.

This flow carries heat towards the Arctic and is an integral part of the North Atlantic thermohaline circulation (THC), which is projected to weaken due to global warming (Collins et al., 2013). It has therefore long been an ambition to monitor its transport of water (volume, mass), heat, and salt. The hydrographic properties (temperature and salinity) of the Faroe Current have been monitored along a section, *section N*, extending northwards from the Faroes since the late 1980s. In the mid-1990s, this section was instrumented with moored Acoustic Doppler Current Profilers (ADCPs) to monitor the transports (Fig. 1b). During and after crossing the IFR, the Atlantic water meets and mixes with colder and less saline water masses, which here are collectively termed *Arctic water*. In this study, we focus on the Atlantic water component of the Faroe Current as it passes through section N.

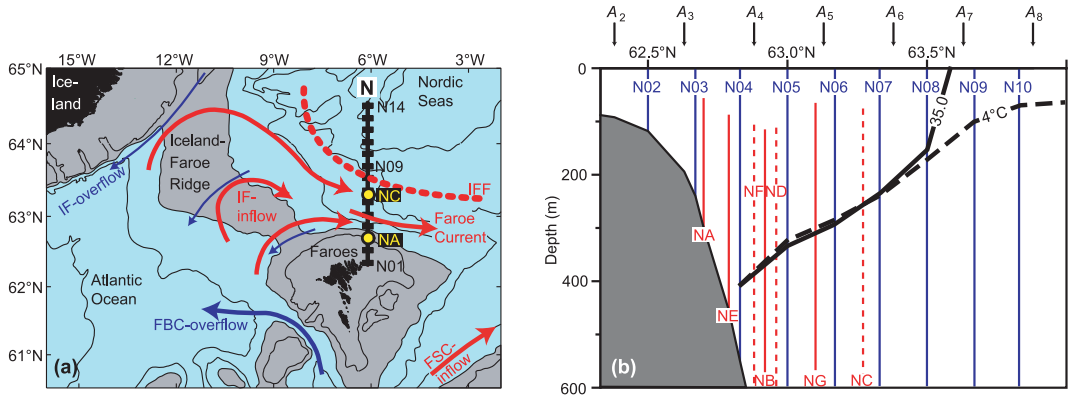

Figure 1. (a) The region between Iceland and the Scottish shelf with gray areas shallower than 500 m. The two main Atlantic inflow branches are indicated by red arrows. The Iceland–Faroe inflow (IF inflow) crosses the IFR, meets colder waters, termed Arctic water, in the Iceland-Faroe Front (IFF), and flows north of Faroes in the Faroe Current. The other main inflow branch (the FSC inflow) is also shown. The black line extending northwards from the Faroe shelf is section N with CTD standard stations N01 to N14 indicated by black rectangles. Yellow circles indicate the innermost (NA) and the outermost (NC) ADCP mooring sites on the section. Blue arrows indicate deep overflow into the Atlantic. **(b)** The southernmost part of section N with bottom topography (gray). Standard CTD stations are indicated by blue lines labeled N02 to N10. ADCP profiles are marked by red lines that indicate the typical range with continuous lines indicating the long-term sites. Altimetry grid points A_2 to A_8 are marked by black arrows and the thick black lines indicate the average depth of the 4 °C isotherm (dashed) and the 35.0 isohaline (continuous) on the section.

A priori, it might seem inappropriate to locate the monitoring section downstream of the IFR rather than on it. The ridge is, however, wide and inflow has been reported to occur over most of its width (Orvik and Niiler, 2002; Jakobsen et al., 2003; Rossby et al., 2009). Strong mesoscale activity and the counterflow of cold overflow water (IF overflow) below the Atlantic water also requires high spatial resolution of velocity as well as temperature and salinity measurements. Monitoring on the IFR would therefore require a prohibitively large number of moorings, which would have to be protected from fishing gear. The chosen monitoring section, section N, in contrast, has a much more focused inflow, where most of the ADCPs may be deployed sufficiently deep to avoid loss from fishing gear. Only over the relatively narrow Faroe slope is it necessary to protect the ADCPs by bottom mounted frames (sites NA and NE on Fig. 1b).

After some initial experimentation, monitoring started in summer 1997 with an ADCP array with three moorings (NA, NB, and NC). The array has been altered and mooring sites have been changed, but as a whole, it has continued operating since then, although with gaps during annual servicing and due to instrument failure or loss. In parallel, regular CTD (conductivity, temperature, depth) cruises have gathered hydrographic data at standard stations (Fig. 1), usually 3–5 times a year.

Based on the combined CTD and ADCP data sets, time series of volume transport and heat and salt transport were reported in Hansen et al. (2003) for the 1997–2000 period and in Hansen et al. (2010) for the 1997–2008 period. In both cases, the transport values were based on the in situ data (CTD and ADCP), solely, using the methodology described in Hansen et al. (2003). It appeared that there was good correspondence between these in situ based estimates and satellite altimetry (Hátún and McClimans, 2003; Hansen et al., 2010) and it was recognized that better estimates might be made by combining the in situ observations with satellite altimetry.

We have therefore re-analyzed the complete updated data set including both the in situ data and altimetry data from a line of grid points parallel to and close to the monitoring section (Fig. 1b). This task involves a large number of technical issues that will not be detailed here. These details are described in a Supplementary document, which we will refer to repeatedly. In this paper, we focus on the main results from the analysis, which are the time series of volume, heat, and salt transport by the Atlantic water component of the Faroe Current. We report average values and estimate seasonal variations, but the main aim is to resolve, whether any of the transport series exhibit overall trends over the observational period, and to quantify them.

2 Material and methods

All the in situ observations (available at www.envofar.fo) were collected along section N (Fig. 1). Altimetry data are selected along a line following longitude 6.125° W, which is so close that we consider it to be along the same section.

2.1 Hydrographic observations

Fourteen standard stations, labeled N01 to N14, are located equidistantly along section N following 6.083° W with a separation of 10 nautical miles from N01 at 62.333° N to N14 at

Table 1. Main characteristics of the measurements at the seven ADCP sites. For the four long-term deployment sites, the table also lists averages and standard deviations of the extrapolated eastward surface velocity.

Site	Latitude	Bottom depth (m)	Period	Duration (days)	Average ($cm\,s^{-1}$)	SD ($cm\,s^{-1}$)
NA	62.70° N	300	Jan 1996–May 2014	6311	18	15
NE	62.79° N	455	Jul 2000–May 2011	2729	25	19
NB	62.92° N	925	Jun 1997–May 2014	5775	22	20
NG	63.10° N	1815	Jul 2000–May 2014	4436	12	21
NF	62.88° N	700	Jul 2000–Jun 2001	343		
ND	62.96° N	1280	Nov 1997–Jun 1998	213		
NC	63.27° N	1730	Jun 1996–Jun 2000	1400		

64.5° N (N14 is at longitude 6.000° W). Properties at these stations are labeled by the index j ($j = 1$ to 14). Typically, the section has been occupied on four cruises each year since 1988 although bad weather and other conditions have prevented complete coverage in some cases. Thus, some stations have been occupied almost a hundred times, but others considerably less often, especially in the northernmost part.

We use quality-controlled and calibrated CTD data averaged to meter intervals with a main focus on data between stations N02 and N11, which contain that part of the section through which the Atlantic water passes. Accuracy is better than 0.01 °C for temperature and 0.01 for salinity throughout the period although salinity spikes in strong thermoclines may exceed this threshold prior to 1997 when the high quality (SeaBird 911+) CTD model was first acquired.

2.2 In situ current velocity observations

Between January 1996 and May 2014, ADCPs have been moored at seven different sites along the section (Table 1). Each site is labeled by a two-letter code beginning with "N". At two sites (NF and ND), only single deployments were made. The other sites have had repeated deployments, with moorings usually deployed in summer one year and recovered the year after. Thus, there are typically gaps of 2–4 weeks every summer.

The most complete coverage has been when all four "long-term" sites (NA + NE + NB + NG) were occupied, from summer 2000 to summer 2001 and from summer 2004 to summer 2011. At most sites, the ADCPs have been deployed in the top of traditional moorings at sufficient depth to prevent loss from fishing gear. At the shallow sites, NA and NE, it has been necessary to put the ADCPs into protective buoyant frames attached by acoustic releases to concrete anchors deployed on the bottom (Fig. S2.2.1 in the Supplement). The ADCPs have typically pinged every 20 min (single pings).

After extensive editing and quality control, the data have been averaged to daily values with accuracy $\approx 0.2\,cm\,s^{-1}$. From the observations, we find that the shape of the ADCP profiles at each site is very consistent so that the ratio between eastward velocities at two different depths is relatively constant in time (Fig. 2). Using observed and extrapolated values for this ratio (Fig. 2), we have extrapolated all the profiles from the long-term sites to the surface. We also use the bottom temperature measured by the ADCP temperature sensor at site NE, T_{NE}, close to the typical boundary between Atlantic and Arctic water masses (Fig. 1b). This sensor may have offsets several tenths of a degree, but that is adequate for our purpose.

2.3 Satellite altimetry

Daily averaged altimetry was selected from the global gridded (0.25° × 0.25°) AVISO+ sea level anomaly (SLA) field produced by Ssalto/Duacs and distributed by Aviso with support from Cnes (http://www.aviso.altimetry.fr). We have used the DT MSLA "all sat merged" data set (http://www.aviso.altimetry.fr/fileadmin/documents/data/tools/hdbk_duacs.pdf). SLA values were selected for 8 grid points, which we label A_1 to A_8, along 6.125° W from 62.125 to 63.875° N (Fig. 1b). We use the index k ($k = 1$ to 8) to identify these points. For each of these points, we have sea level anomalies $H_k(t)$ for 7791 days from 1 January 1993 to 1 May 2014. An empirical orthogonal function (EOF) analysis on the SLA values from these eight points revealed that the first two modes explained 95 % of the variance with 87 % in the first mode (Fig. 3). The associated principal components (temporal variation) are denoted $PC_1(t)$ and $PC_2(t)$, respectively. The EOF modes also revealed that the flow variations are confined to the region north of A_2, which is the region we will focus on.

At timescales exceeding a few days, we expect approximate geostrophic balance, so that the horizontally averaged eastward surface ($z = 0$) velocity $U_k(0,t)$ between grid points A_k and A_{k+1} is proportional to the difference in absolute sea level height (SLH) between the two points. The SLA values do not represent absolute SLH (above the geoid), but rather the anomaly. Surface velocities derived from SLA differences between two grid points are therefore also anomalies, but may be made absolute by adding a constant U_k^0 for

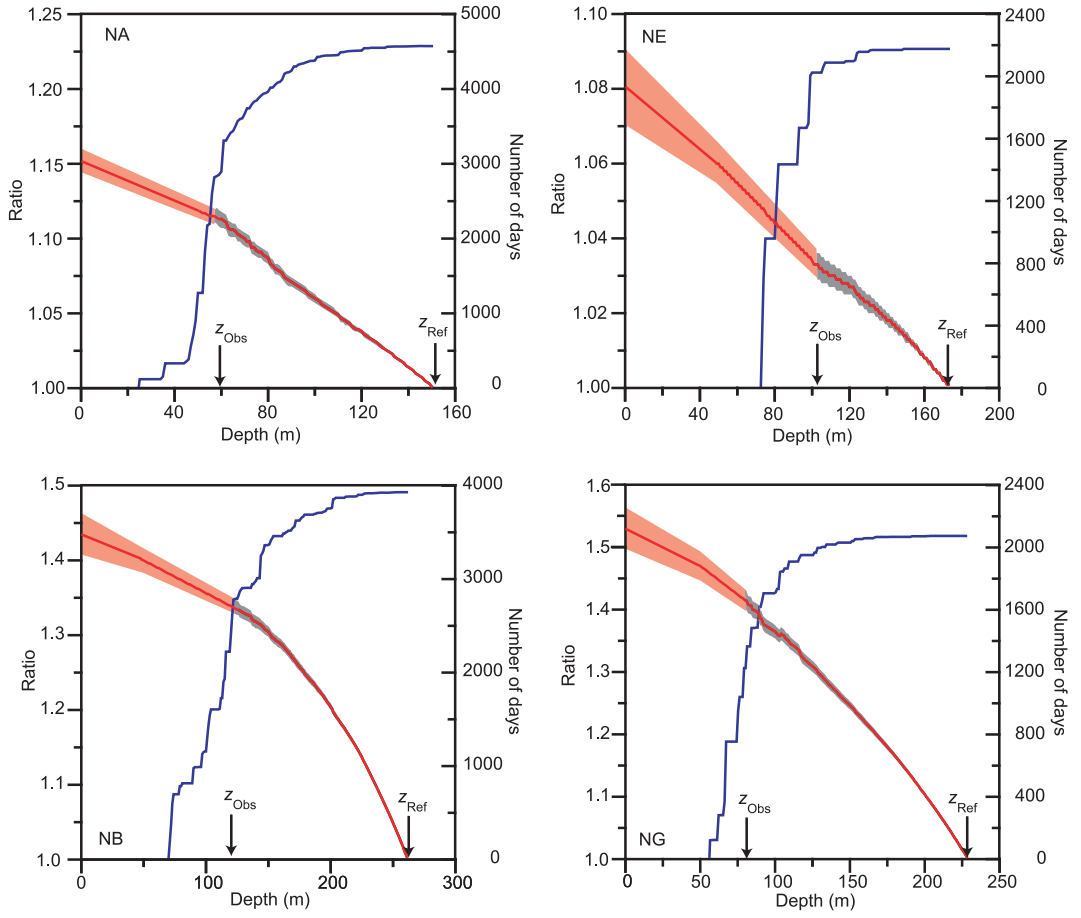

Figure 2. Vertical variation of eastward velocity for the long-term ADCP sites. Each panel shows for one of the long-term ADCP sites, the number of days with data at each depth (blue curve, right scale) and the ratio $U(z,t)/U(z_{\mathrm{Ref}},t)$ (red curve, left scale). Here, $U(z,t)$ is eastward velocity at depth z for time t and z_{Ref} is the depth, up to which all profiles from the site are complete. Profiles with $|U(z_{\mathrm{Ref}},t)| < 10\,\mathrm{cm\,s^{-1}}$ are excluded. From z_{Ref} up to the depth z_{Obs}, the ratio represented by the red curve is the average ratio based on observed ADCP profiles and the shaded gray area is ± one standard error. Above z_{Obs}, graphical extrapolation is applied up to 50 m depth. From there to the surface, the red curve is based on average geostrophic profiles. The shaded red area is graphically extrapolated from the gray area and indicates uncertainty.

each interval:

$$U_k(0,t) = \frac{g}{f \cdot L} \cdot \left[H_k(t) - H_{k+1}(t)\right] + U_k^0, \tag{1}$$

where g and f are gravity and Coriolis parameter, respectively, and L is the distance between the altimetry grid points. The constants U_k^0 for each altimetry interval could be determined from the mean dynamic topography (MDT), available from AVISO, but this would have given a surface current that was broader and considerably weaker than indicated by our in situ observations, especially between A_3 and A_5, where most of the Atlantic water transport occurs (Fig. S2.4.4). Instead, we use values for U_k^0 that are determined from ADCP data and average geostrophic profiles that are derived from the CTD data as elaborated in Sect. 3.1.

2.4 Combining ADCP and altimetry to generate velocity at depth

Once calibrated by Eq. (1), the altimetry data provide us with a time series of horizontally averaged eastward surface velocity $U_k(0,t)$ for each altimetry interval A_k to A_{k+1}. To find the horizontally averaged velocity $U_k(z,t)$ for interval k at depth z, we multiply the surface velocity $U_k(0,t)$ by a function $\varphi_k(z,t)$, which we term the *relative profile*:

$$U_k(z,t) = U_k(0,t) \cdot \phi_k(z,t). \tag{2}$$

If, in a certain period, there is one ADCP that is considered to represent the altimetry interval k, then we may assume that:

$$\phi_k(z,t) = u_{\mathrm{ADCP}}(z,t)/u_{\mathrm{ADCP}}(0,t), \tag{3}$$

as long as u_{ADCP} $(0,\ t)$ is not too close to zero. Much of the time, we have to replace $\varphi_k(z,t)$ by an average relative profile $\Phi_k(z)$ for each interval, however. The average relative profiles are based on average ADCP profiles and on average geostrophic profiles, calculated from the CTD data (Fig. S3.2.2).

2.5 Calculation of transport time series

With the eastward surface velocity $U_k(0,t)$ determined from calibrated altimetry by Eq. (1) and its vertical variation $U_k(z,t)$ given by Eq. (2), time series of volume transport, $Q(t)$, between grid points A_2 and A_8, may be determined as:

$$Q(t) = \sum_{k=2}^{7}\sum_{z=1}^{600} U_k(z,t)\cdot W_k(z,t), \tag{4}$$

where $W_k(z,t)$ is the width of the interval from A_k to A_{k+1} at depth z and time t. If we want to integrate down to 600 m all along the section, then $W_k(z,t) = L$, the distance between grid points, for all k, z, and t, except where the bottom is shallower than 600 m. More generally, we may wish to integrate down to a certain boundary (e.g., the 4 °C isotherm) that varies in depth along the section and also with time. In that case, we can write $W_k(z,t) = L\cdot r_k(z,t)$ where $r_k(z,t)$ is the fraction (between 0 and 1) of the width of altimetry interval k at depth z that is above the boundary or bottom at time t.

To calculate heat transport relative to a specified reference temperature T_{Ref}, we use:

$$Q_{\mathrm{Heat}}(t) = \rho\cdot C_{\mathrm{H}}\cdot\sum_{k=2}^{7}\sum_{z=1}^{600}[T_k(z,t)-T_{\mathrm{Ref}}]\cdot U_k(z,t)\cdot W_k(z,t), \tag{5}$$

where ρ is density, C_{H} is the specific heat, and $T_k(z,t)$ is the temperature at depth z and time t, horizontally averaged from A_k to A_{k+1}.

The salt transport through section N by Atlantic water is well defined in an absolute sense. Every cubic meter passing across the IFR with a practical salinity S represents an input of salt to the Nordic Seas (Fig. 1a) equal to $\rho\cdot C_{\mathrm{S}}\cdot S$ kg where C_{S} is a (approximately constant) factor converting from practical to absolute salinity. The salt transport, relative to some specified reference salinity S_{Ref}, is therefore given by:

$$Q_{\mathrm{Salt}}(t) = \rho\cdot C_S\cdot\sum_{k=2}^{7}\sum_{z=1}^{600}[S_k(z,t)-S_{\mathrm{Ref}}]\cdot U_k(z,t)\cdot W_k(z,t). \tag{6}$$

3 Results

The basic results of this study are the characteristics of the velocity field, generated by combining ADCP and altimetry data, and the characteristics of the temperature and salinity fields, mainly based on the CTD observations. By combining these results, we can produce continuous time series of Atlantic water characteristics (T and S) and spatial extent on the section and we can simulate distributions of velocity, temperature, and salinity with reasonable accuracy. Together, these series allow us to generate the main results: continuous time series of volume, heat, and salt transport for the whole altimetry period.

3.1 Velocity distribution on the section

The average velocity profiles from the ADCPs and from geostrophy (Fig. 4) are compatible. We also find that the relative profiles – the $\varphi_k(z,t)$ functions introduced in Sect. 2.4 – are consistent in shape. This is verified by correlating the extrapolated eastward surface velocity and the vertically averaged eastward velocity for individual long-term ADCP sites. For weekly averages, we find correlation coefficients between 0.94 and 0.98 (Table S3.2.1 and Fig. S3.2.1 in the Supplement). This indicates that replacing $\varphi_k(z,t)$ by the average relative profile $\Phi_k(z)$ in Eq. (2) should generally be a good approximation.

After extrapolation to the surface, average eastward velocities for the four long-term ADCP sites (Table 1) combined with more scattered observational evidence in the Faroe shelf region give a consistent picture of the horizontal variation of the average eastward surface current (black curve in Fig. 5). Farther north on the section, average geostrophic profiles combined with deep current measurements complete this picture (blue lines in Fig. 5). By averaging over each altimetry interval, this leads to values for U_k^0 for $k = 2$ to 7 (red line in Fig. 5).

3.2 Temperature and salinity distributions

In the CTD data set, there are 78 cruises with complete coverage from station N02–N11 in the period 1993–2013. The average temperature (Fig. 6a) and salinity (Fig. 6c) distributions on the section illustrate the characteristic difference between the warm and saline Atlantic water and the colder and less saline Arctic water masses except that seasonal heating blurs the water mass characteristics in the uppermost layers in the northern part of the section (Fig. S4.1).

Seasonal heating is also indicated by a relatively high standard deviation of temperature in the near-surface layer, but the highest standard deviations for both temperature and salinity are in the pycnocline region (Fig. 6b and d) and illustrate variations in Atlantic water extent.

To a large extent, the variations in hydrographic properties may be seen as composed of three different contributions: (1) interannual variations in the temperature and salinity of the Atlantic water, (2) seasonal variations, especially of temperature near the surface, and (3) variations in the extent of the Atlantic water on the section downwards and northwards

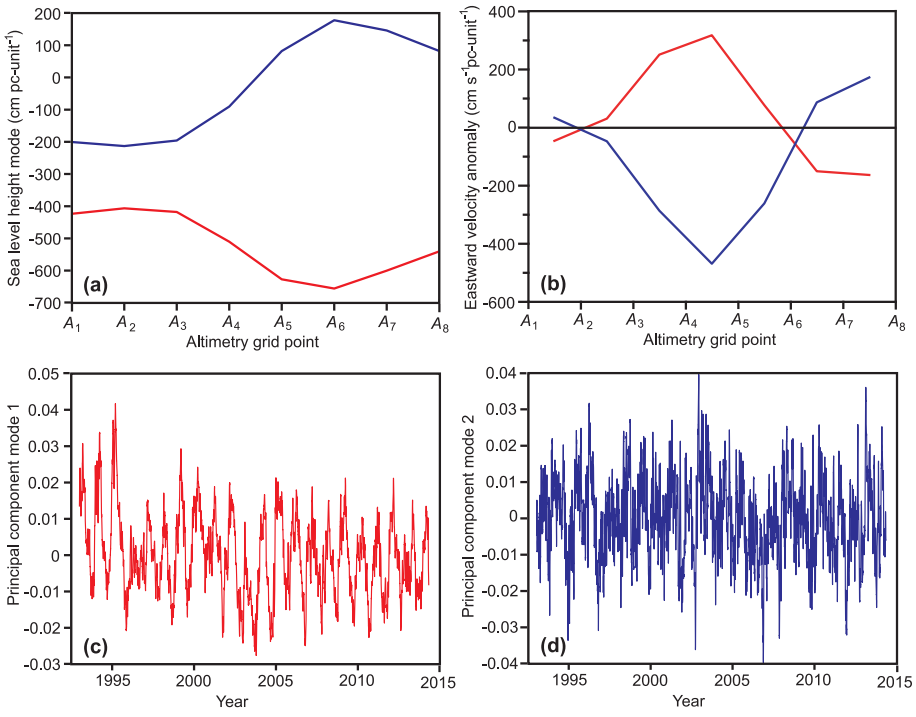

Figure 3. The first two EOF modes of the altimetry data and their principal components. **(a)** SLA mode 1 (red) and 2 (blue). **(b)** The eastward surface velocity anomaly associated with SLA mode 1 (red) and 2 (blue) using Eq. (1) with $U_k^0 = 0$. **(c)** Principal component of SLA mode 1, $\mathrm{PC}_1(t)$. **(d)** Principal component of SLA mode 2, $\mathrm{PC}_2(t)$.

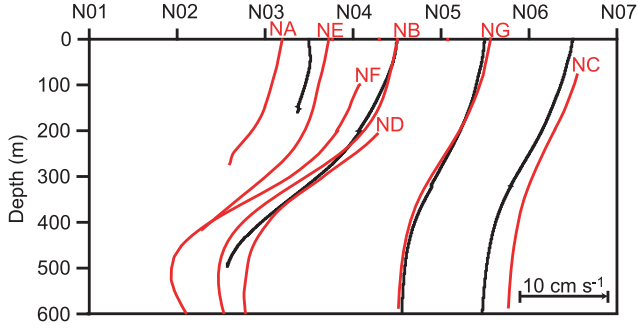

Figure 4. Average eastward geostrophic velocity profiles (black) between each pair of neighboring standard stations from N03 to N07 and eastward ADCP velocity profiles from all sites (red). The surface expressions of the geostrophic profiles are located in the middle of the associated station pairs. For the long-term sites, the profiles have been extrapolated to the surface where they are located at the ADCP positions.

(frontal variations). In the next three sections, we try to estimate these.

3.2.1 Atlantic water temperature and salinity

As seen in Fig. 6, the southernmost stations over the shelf and inner slope are usually dominated by Atlantic water (reddish colors) and this region has also been most frequently sampled in the CTD cruises. We have therefore generated time series of Atlantic water temperature and salinity by averaging between 100 and 150 m depth at station N03. These time series are termed $T_\mathrm{A}(t)$ and $S_\mathrm{A}(t)$.

For both of these parameters, we have extracted the seasonal (Fig. S4.5.3) and the interannual variations (Fig. 7) using an iterative procedure (Appendix B in the Supplement). The Atlantic water temperature increased about 1 °C from 1993 to 2003, after which there are no consistent trends. The salinity changes of the Atlantic water parallel the temperature changes with an overall increase of about 0.1.

3.2.2 Atlantic water extent on the section

In this study, we define Atlantic water to be water that has recently crossed the IFR. In order to include only this component of the volume, heat, and salt transports, Eqs. (4)–(6) require that we are able to establish a boundary between the Atlantic and the Arctic domain on the section at any time. In reality, this boundary will be diffuse and different methods may be used to solve this (Hansen et al., 2003) but they all suffer from lack of sufficiently comprehensive hydrographic observations.

In the southernmost part of the section, we find fairly undiluted Atlantic water of temperature ≈ 8 °C in the upper layers and Arctic water with temperature ≈ 0 °C at depth (Fig. 6a). The 4 °C isotherm therefore ought to be an approximate

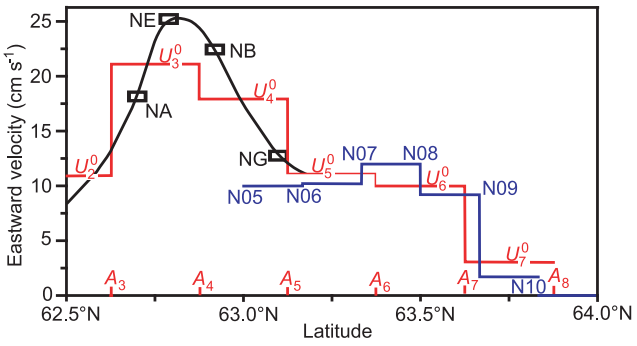

Figure 5. Values for the altimetry offset U_k^0 (red line) plotted together with average values for eastward surface velocity from the four long-term ADCP sites (rectangles) and from average geostrophy (Table S2.4.3) (blue line). South of site NA, the velocity is estimated from various scattered observations (Fig. S2.4.4). The black curve shows a graphical interpolation from this region and between ADCP sites and values for U_2^0, U_3^0, and U_4^0 are averaged from these. The value for U_5^0 is a combination of ADCP site NG and geostrophy between N06 and N07 (blue line). Values for U_6^0 and U_7^0 are based on geostrophy combined with deep current measurements (Table S2.4.3).

boundary between the Atlantic and the Arctic domain on the section. The amount of Arctic water that has been mixed into the area above this isotherm should be similar to the amount of Atlantic water that has been mixed below it. The depth of this isotherm at station j and time t is denoted $D_j(t)$.

From direct observations, we only know the depth of this isoline at the times of CTD cruises. As shown by Hátún et al. (2004), the temperature (and salinity) field is, however, linked to the velocity field, which again is linked to the altimetry. To investigate this, all CTD cruises since 1993 were analyzed to find the depth of the 4 °C isotherm at stations N04–N11. No clear overall trend or seasonal variation were evident (Fig. S4.2.1). These depth values were then correlated with various parameters that might be considered to influence isotherm depth (Table S4.2.1).

For most stations, the altimetry data provided the best indicator of the 4 °C isotherm depth and a multiple linear regression on two separate altimetry parameters could explain between 56 and 65 % of the variance in 4 °C isotherm depth for the five stations from N05 to N09. For stations N10 and N11, the explained variance decreased to 47 and 42 %, respectively (Table S4.2.1).

For station N04, only 30 % of the 4 °C isotherm depth variance could be explained by altimetry and ADCP velocity data, solely, but the inclusion of bottom temperature observed at ADCP site NE increased the explained variance to 58 %. This site is located where the thermocline typically intersects the bottom (Fig. 1b) and the bottom temperature exhibits large variations – even on monthly timescales (Fig. S4.3.1) – that indicate Atlantic water extent in the area.

Using the coefficients from these regression analyses, the depth of the 4 °C isotherm at most stations, $D_j(t)$, may be simulated with reasonable accuracy for every day with altimetry data, i.e., since 1 January 1993. Especially for days in this period with bottom temperature measurement at site NE, we can simulate the 4 °C isotherm depth from its intersect with the Faroe slope north to station N09, explaining more than half of its total variance.

At station N09, the isotherm already approaches the surface and has diverged from the 35.0 isohaline (Fig. 1b). Here, temperature is no longer a good indicator of Atlantic water extent. To simulate the northern boundary of the Atlantic water extent, we instead seek to simulate the location of the 35.0 isohaline in the near-surface layer (Fig. 1b). This was also explored by multiple linear regressions on various altimetry parameters using CTD observations from the 1997 to 2013 period, for which the salinity data have the best quality.

Based on this, an algorithm was developed that allowed simulation of the latitude of the 35.0 isohaline at 100 m depth from altimetry data, explaining 44 % of its variance (Fig. S4.4.1). This is used to determine the northern boundary of the Atlantic water extent for the top 100 m layer.

As elaborated in Sect. 3.6, the choice of boundary for Atlantic water extent is a dominant source of uncertainty for average transport estimates. Since the regression equations for $D_j(t)$ include mainly altimetry parameters (Table S4.2.2), our results are not, however, very sensitive to changes in the Atlantic water properties. Thus, this choice should not introduce appreciable uncertainties to the temporal variations and trends of the transport series.

3.2.3 Simulating daily temperature and salinity fields

With continuous simulation of the boundary of Atlantic water extent, Eqs. (1)–(4) allow calculation of the volume transport of Atlantic water, but for heat and salt transport, we need continuous simulations of temperature and salinity distributions on the section, as well. To develop these, we used the CTD data from all the 78 cruises 1993–2013 that had complete coverage from station N02–N11. We found that the temperature distribution is well explained as a linear combination of a seasonal signal, the Atlantic water temperature, $T_A(t)$ (Fig. 7) and the depth of the 4 °C isotherm $D_j(t)$. For stations N04 to N11, the temperature $T_j(z,t)$ at station j, depth z, and time t is expressed as:

$$T_j(z,t) = T_j^{\mathrm{Seas}}(z,t) + a_j(z)\cdot T_A(t) + b_j(z)\cdot D_j(t) + c_j(z). \quad (7)$$

In this expression, $T_j^{\mathrm{Seas}}(z,t)$ is a sinusoidal seasonal variation determined by regression (Fig. S4.6.1). The regression coefficients a, b, and c depend on the station number (latitude) and depth, but not on time. For stations N02 and N03, where the 4 °C isotherm would have been below the bottom, we use the principal component $\mathrm{PC}_1(t)$ from the altimetry

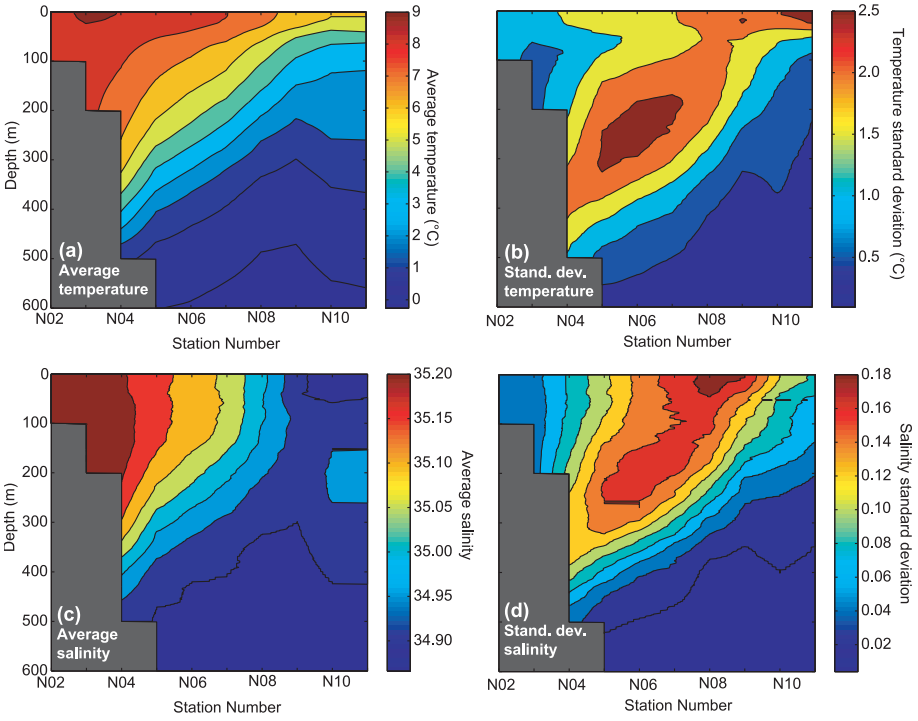

Figure 6. Hydrographic conditions on section N based on 78 CTD sections in the period 1993 to 2013. **(a)** Average temperature; **(b)** standard deviation of temperature; **(c)** average salinity; **(d)** standard deviation of salinity. Gray areas indicate the bottom.

instead of $D_j(t)$ in Eq. (7). The explanatory power of this expression varies across the section, but over the average Atlantic water extent, Eq. (7) explains 61 % of the total variance, on average (Fig. S4.6.2).

For salinity, the seasonal variation is less pronounced (Fig. S4.8.1). To simulate the salinity at station j ($j = 4$ to 11), depth z, and time t, $S_j(z,t)$, we therefore use the expression:

$$S_j(z,t) = d_j(z) \cdot S_A(t) + e_j(z) \cdot D_j(t) + f_j(z), \quad (8)$$

where $S_A(t)$ is the salinity of the Atlantic water (Fig. 7) and d, e, and f are regression coefficients. At stations N02 and N03, $D_j(t)$ is again replaced by $PC_1(t)$. On average over the average Atlantic water extent, Eq. (8) explains 47 % of the total variance in the observed salinity (Fig. S4.8.2).

3.3 Volume transport

3.3.1 Total volume transport

Once appropriate choices for the relative profile functions $\varphi_k(z,t)$ and $\Phi_k(z)$ have been made for each altimetry interval k (Table S5.3.1), Eqs. (1)–(4) allow calculation of volume transport, as long as the $W_k(z,t)$ functions are specified. As a test case, we consider the volume transport from the surface to 500 m and from N02 (midway between A_2 and A_3) out to A_8 (Fig. 1b), which we here denote total volume transport. This requires $W_2(z,t) = L/2$ and $W_k(z,t) = L$ for $k = 3$ to 7 for all depths $z = 1$ to 500 (or bottom where shallower). Outside of this area $W_k(z,t) = 0$.

From 1 January 1993 to 1 May 2014, there are 223 weeks for which we have altimetry data, as well as data from all four long-term ADCP sites (NA, NE, NB, and NG). For these weeks, we can compare transport estimates based on the instantaneous relative profiles $\varphi_k(z,t)$ with estimates based on the average relative profiles $\Phi_k(z)$. For monthly (4-week) averages, the correlation coefficient between these two estimates is 0.94 with an average difference of 0.03 Sv and a rms (root-mean-square) difference of 0.3 Sv (Table S5.3.2). This is 6 % of the average volume transport and well below its estimated uncertainty (Sect. 3.6).

This implies that the average relative profiles $\Phi_k(z)$ may be used instead of $\varphi_k(z,t)$ without appreciable error. More importantly, it implies that the $\Phi_k(z)$ functions, which do not depend upon time, give a sufficiently good representation of the velocity variation, vertically, to allow accurate transport calculation whenever the surface velocity is known. As a consequence, we can calculate transports; not only for periods with good ADCP coverage, but for the whole altimetry period since 1 January 1993.

3.3.2 Volume transport of Atlantic water

The total volume transport down to 500 m depth, calculated above, includes water of Arctic origin. To obtain an estimate of Atlantic water volume transport only, values for $W_k(z,t)$

Table 2. Average (1 January 1993–1 May 2014) volume transport between N02 and A_8 above either a fixed depth of 500 m, a selected average isotherm ($T =$), or a selected average isohaline ($S =$) in the hydrographic fields.

Isoline	$D = 500$ m	$T = 2$ °C	$T = 3$ °C	$T = 4$ °C	$T = 5$ °C	$T = 6$ °C	$T = 7$ °C	$S = 34.9$	$S = 35.0$	$S = 35.1$
Transport (Sv)	4.66	4.46	4.28	4.05	3.76	3.35	2.70	4.56	3.95	3.26

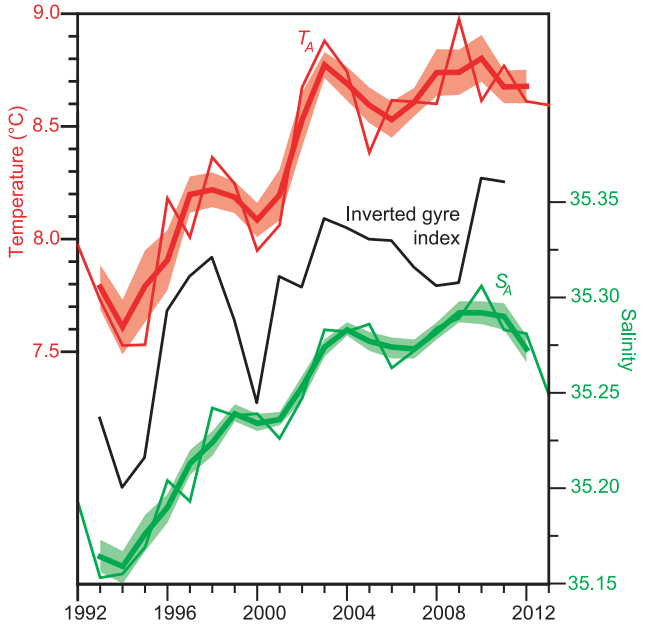

Figure 7. Interannual variation of Atlantic water temperature, T_A (red) and salinity, S_A (green) and of the inverted subpolar gyre index (black). For T_A and S_A, the figure shows annually averaged deseasoned values (thin curves) and 3-year running mean of deseasoned values (thick curves) with background colors indicating ± one standard error over each 3-year period. The inverted (for easier comparison) gyre index (updated from Larsen et al., 2012) is shown in a relative scale.

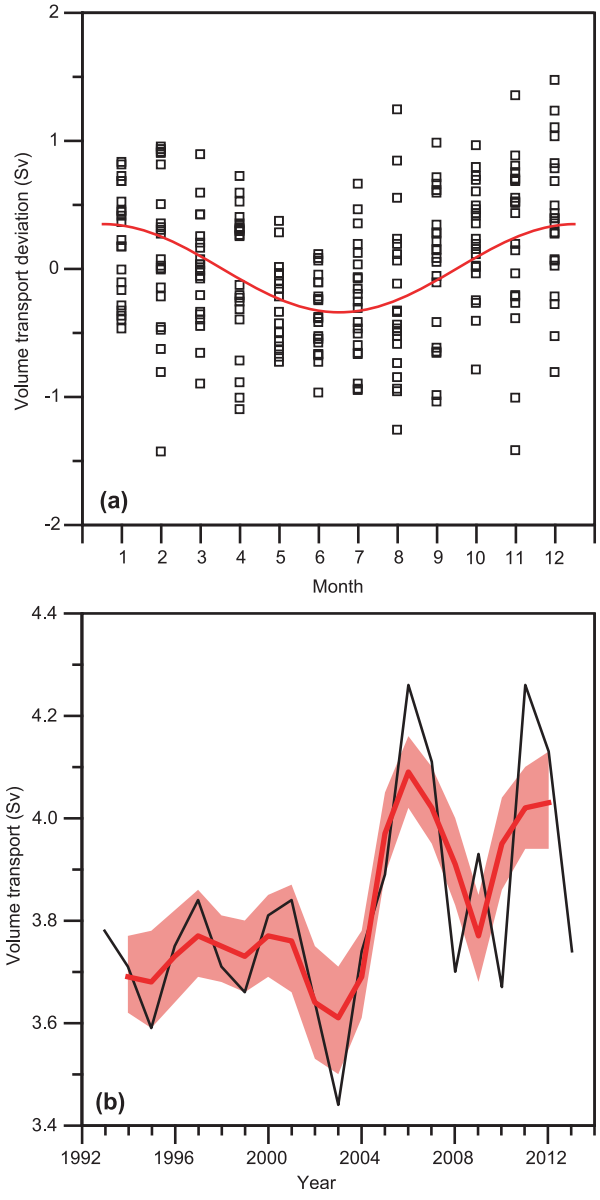

Figure 8. Seasonal **(a)** and interannual **(b)** variations of Atlantic water volume transport 1993–2013. **(a)** Each square represents transport deviation from the 3-year running mean for 1 month. The red curve represents the iteratively determined sinusoidal seasonal fit (Appendix B in the Supplement). **(b)** Annually averaged transport (black curve) and 3-year averaged transport (red curve) with the red background representing ± one standard error over each 3-year period.

have to be specified, so that the transport estimate only includes water that has crossed the IFR recently. One way to do that is to assume that the Atlantic water on the section is bounded by a specified isotherm or isohaline. Table 2 compares volume transports using different choices for the bounding isoline and assuming that it remains fixed to its average depth.

In reality, the isolines do not stay at fixed depths and the deep boundary of the Atlantic water extent, as well as its northward surface boundary, vary in time. As argued in Sect. 3.2.2, we use the 4 °C isotherm (or bottom where shallower) to define the deep boundary and the 35.0 isohaline to define the northward boundary in the 0–100 m depth layer. Both of these may be simulated for each day in the altimetry period, as discussed in Sect. 3.2.2 (Table S4.2.2 and Eq. S4.4.2), allowing daily estimates of $W_k(z,t)$.

The data set, thus, allows daily estimates of Atlantic water volume transport, but the algorithms are developed from

regression analyses, that will give better estimates for longer averaging periods. Also, we expect the quality of the altimetry data, and even the validity of geostrophy, to increase with the averaging period. In the following, we therefore will consider monthly averaged transport values.

To study the variations in Atlantic water volume transport, monthly averages were calculated for the 1993–2013 period. The overall average was 3.82 Sv and an iterative procedure (Appendix B in the Supplement) was used to extract seasonal (Fig. 8a) and interannual (Fig. 8b) variations. In contrast to previous studies (Hansen et al., 2003, 2010), there is an indication of a seasonal variation with maximum flow around the turn of the year. The maximum correlation coefficient in the fit with the sinusoidal signal was, however, not very high and the seasonal amplitude was below one tenth of the average (Table 3). On average, more than 70 % of the Atlantic water transport occurs between A_3 and A_5 (Fig. S5.4.1).

As previously noted (Hansen et al., 2010), the annually averaged Atlantic water volume transport had a minimum in 2003, but since then, it seems to have been at a generally higher level than before 2003 (Fig. 8b). A linear regression on time reveals an increasing trend: $0.016 \pm 0.015\,\mathrm{Sv\,yr^{-1}}$ (Table 3) with a 95 % confidence interval (Sect. 3.6).

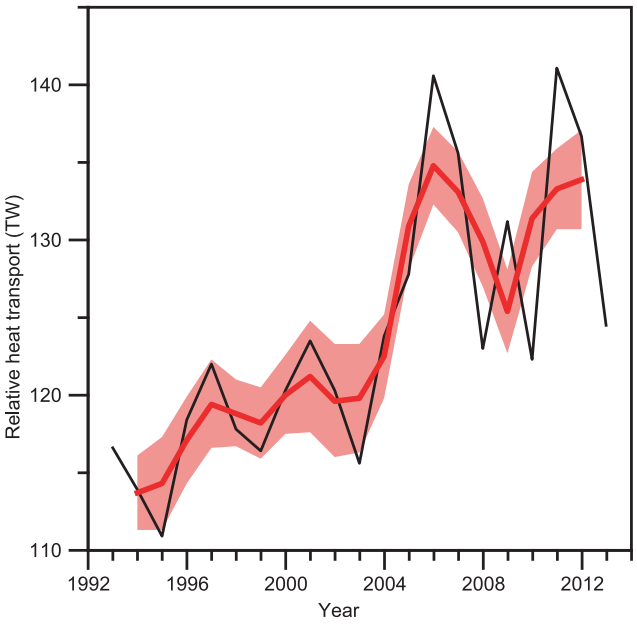

Figure 9. Interannual variation of relative (to 0 °C) heat transport 1993–2013. Annually averaged transport (black curve) and 3-year averaged transport (red curve) with the red background representing ± one standard error over each 3-year period.

3.4 Heat transport

The heat delivered by any inflow branch to the Arctic Mediterranean (Nordic Seas and Arctic Ocean) equals the heat lost by the water before it exits again. Thus, the heat transport is proportional to the temperature of the inflowing water minus the temperature of the water when it returns back to the Atlantic Ocean either as overflow or as surface outflow in the East Greenland Current or through the Canadian Archipelago. Thus, the heat transport of the Faroe Current is only well defined if we know the average outflow temperature, which is the appropriate reference temperature, T_{Ref} in Eq. (5). The detailed pathways of the various inflow branches are not well known, but most likely the average outflow temperature of the water that entered in the Faroe Current is close to 0 °C (Hansen et al., 2008). We therefore calculate heat transport relative to $T_{\mathrm{Ref}} = 0\,^{\circ}\mathrm{C}$ and term this relative heat transport.

As noted in Sect. 3.2.3, we may simulate daily temperature fields $T_j(z,t)$ for the whole altimetry period with reasonable accuracy. This allows us to use Eq. (5) to calculate relative heat transport, but it is not obvious that the 4 °C isotherm is the appropriate boundary in this case, since the Atlantic water that by mixing has been cooled below 4 °C originally carried more heat than the Arctic water that has been heated above 4 °C. Instead, we should use a colder isotherm as Atlantic water boundary for heat transport calculation. The cold waters close to the Atlantic water boundary do, however, not transport much heat, especially since average velocities are low. Consistent with that, we also find that the average relative heat transport is not very sensitive to the exact definition of Atlantic water extent (Table S6.1.1).

As for the volume transport, the relative heat transport does not exhibit a very pronounced seasonal variation (Fig. S6.1.2), and the seasonal amplitude is about 10 % of the average (Table 3). For the interannual variation, Fig. 9 clearly indicates an increasing trend, which is $1.0 \pm 0.5\,\mathrm{TW\,yr^{-1}}$, from a linear regression on time. This is highly significant and not very dependent on the boundary chosen for Atlantic water extent (Table S6.1.1). Over the 20-year interval from 1993 to 2013, this corresponds to an increase in relative heat transport of ∼ 18 %. Most of the change occurred from 2003 to 2006.

3.5 Salt transport

The salt transport through section N by Atlantic water is given by Eq. (6). Eventually, this salt is returned to the Atlantic by the overflows and surface outflows, but the returning water has been diluted by added freshwater and the low-salinity Pacific inflow through the Bering Strait. A rough budget estimate indicates that the salinity is reduced by about 1 on average (Hansen et al., 2008), but the overflows, which will return a large fraction of the Faroe Current, are more saline. The average salinity of the neighboring (Fig. 1a) Faroe Bank Channel overflow is ∼ 34.93 (Hansen and Østerhus, 2007).

In addition to the absolute salt transport, which we get by choosing the reference salinity $S_{\mathrm{Ref}} = 0$, it may therefore be

Table 3. Characteristics of transport time series. Averages for the 1993–2013 period. Trends are based on a linear regression of annual averages on time with 95 % confidence intervals. Seasonal variation is determined by an iterative procedure (Appendix B in the Supplement) where "R_{max}" is the maximum correlation coefficient with a sinusoidal seasonal signal, "Ampl." is the seasonal amplitude and "Max." is the day number in the year with maximum value.

Time series	Average	Trend	Seasonal variation R_{max}	Ampl.	Max.
Atlantic water volume transport	3.8 ± 0.5 Sv	0.016 ± 0.015 Sv yr^{-1}	0.34	0.34 Sv	1
Heat transport relative to 0 °C	124 ± 15 TW	1.0 ± 0.5 TW yr^{-1}	0.39	13 TW	307
Absolute salt transport	$(140 \pm 30) \times 10^6$ kg s^{-1}	$(1.9 \pm 0.7) \times 10^6$ kg s^{-1} yr^{-1}	0.33	14×10^6 kg s^{-1}	14
Salt transport relative to 34.93	$(900 \pm 140) \times 10^3$ kg s^{-1}	$(33 \pm 7) \times 10^3$ kg s^{-1} yr^{-1}	0.33	91×10^3 kg s^{-1}	352

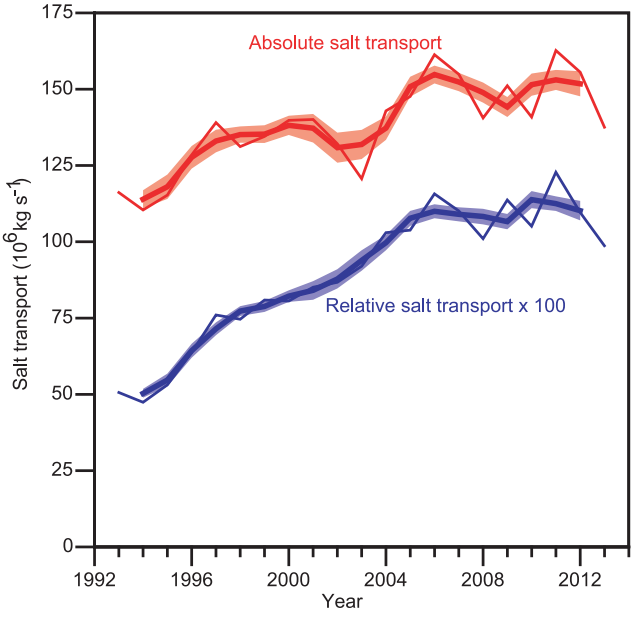

Figure 10. Interannual variation of absolute (red) and relative to 34.93 (blue) salt transport 1993–2013. Annually averaged transports (thin lines) and 3-year averaged transports (thick lines) with the background representing ± one standard error over each 3-year period. The values for relative salt transport have been multiplied by 100 to fit the same scale as the absolute salt transport.

appropriate to consider the transport relative to some other values for S_{Ref}. Using the simulated values for $S_j(z,t)$ in Eq. (8), time series of salt transport for specified values of S_{Ref} may be generated, but the problem, again, is to distinguish between the Atlantic water and other water masses. This introduces considerable uncertainty into calculations of absolute salt transport, but the salt transport relative to higher salinities is much less sensitive to the boundary chosen for Atlantic water extent (Table S6.2.1). This is reflected in the uncertainties for the average values listed in Table 3.

As for volume and relative heat transport, we can extract the seasonal (Table 3) and an interannual variation (Appendix B in the Supplement) from the salt transport time series. This clearly has an increasing trend whether we consider the absolute transport ($S_{Ref} = 0$), or the transport relative to 34.93 (Fig. 10). A linear regression of annually averaged salt transport on time yields trends that are positive and significantly different from zero for all choices of S_{Ref} (Table S6.2.1) and more significant, the higher the S_{Ref} value. The salt transport relative to $S_{Ref} = 34.93$ more than doubled throughout the observational period (Fig. 10).

3.6 Uncertainty estimates

Many different approximations affect the accuracies of the average transport values reported here and fully objective error estimates are difficult to generate from the available information. For all the transport series, the eastward surface velocities, used to calibrate the altimetry data (Fig. 5), are a critical component and their uncertainties will affect all the transport estimates. The uncertainties in extrapolation of ADCP velocities range between 1 and 3 % (Fig. 2). Interpolating between ADCP sites in the region between A_3 and A_5 adds another 1 % to the average eastward surface velocity (Fig. S2.4.4). This region has most of the average transport ~ 3 Sv and we may estimate an uncertainty of ~ 0.15 Sv for this region. The rest of the section has a smaller average transport ~ 1 Sv, but with higher relative uncertainties. We add another 0.1 Sv for this part to get a total uncertainty of ~ 0.25 Sv from the velocity field. Another uncertainty source for the average volume transport of Atlantic water is the choice of boundary for the Atlantic water extent. From Table 2, choosing the 3 °C isotherm or the 5 °C isotherm instead of the 4 °C isotherm would change the average volume transport of Atlantic water by ~ 0.25 Sv. Adding this to the uncertainty from the velocity field, we get the value 0.5 Sv.

For the average heat transport, we have to include the 0.25 Sv uncertainty from the velocity field, which is equivalent to 7 %, and the uncertainty from the Atlantic water extent is estimated at 3 % (Table S6.1.1). Finally, uncertainty of the Atlantic water temperature (Fig. 7) is assumed to give another 0.15° C equivalent to 2 %, so that the total adds up to ~ 12 % or 15 TW.

For the average salt transport, the importance of the various uncertainty sources varies depending on the choice of reference salinity. For absolute salt transport ($S_{Ref} = 0$), the

assumption of boundary salinity is critical, whereas the uncertainty of Atlantic water salinity becomes more important with high values for S_{Ref}. Combining the various error sources, we estimate an uncertainty of 20 % for absolute salt transport and 15 % for reference salinities close to 34.95.

Most of the uncertainty sources, quoted above, may be seen as biases. Thus, they affect the average transport values, but should not affect the temporal changes in transport appreciably. Any remaining errors should be included in the statistical uncertainties cited for the overall trends of transports (Sects. 3.3–3.5). The statistical uncertainties of the trends are the 95 % confidence limits for the slope of the regression line when annually averaged transport values are regressed on the year using the t-distribution. The only exception derives from possible systematic errors in the altimetry data. If these data were to include artificial overall trends, then the trend in volume transport might be affected, but the trends in relative heat and salt transport would still be robust since they are dominated by the trends in Atlantic water temperature and salinity (Fig. 7).

4 Discussion

The transport time series presented in this study are generated from a number of assumptions and approximations: geostrophy, use of the average relative profiles $\Phi_k(z)$ in Eq. (2), our choice of the 4 °C isotherm and 35.0 isohaline as boundaries for Atlantic water extent, etc. Based on an evaluation of their effects on the results, we find that the chosen method of combining in situ observations with altimetry produces more reliable transport values than estimates based on the in situ data, solely.

We also find that the method allows estimates in periods without in situ velocity measurements as long as there are no major changes in the structure of the velocity field. This justifies the validity of our continuous transport series for the whole altimetry period. One advantage of this is that we now have transport estimates also for the summer months with the ADCPs on land for servicing, especially for June.

4.1 Comparison with other estimates of the IF inflow

The overall average Atlantic water transport for 1993–2013, estimated in this study (3.8 ± 0.5 Sv) is slightly higher than the previously reported average transport (3.5 ± 0.5 Sv), based on a subset of the same in situ data, but without using altimetry data (Hansen et al., 2003, 2010). The difference is within the uncertainty bounds, however. Comparing monthly averaged volume transport estimates, the best correspondence is for the 57 months when all four long-term ADCPs were in operation (Fig. S5.5.1), but even in that case the correlation coefficient is only 0.58 (Table S5.5.1). Considering the approximations made in the old in situ based estimates, we conclude, however, that the new transport values should be more realistic than the old ones (Sect. S5.5).

In addition to our own old estimates, there are not many observational transport estimates of the IF inflow, but Rossby and Flagg (2012) have reported estimates based mainly on vessel-mounted ADCP observations from a ferry making regular tracks between Faroes and eastern Iceland. Their values were updated by Childers et al. (2014) who reported an average inflow of 4.6 ± 0.5 Sv across the IFR. Their value is higher than ours, although the uncertainty intervals overlap, but differences in definitions and timing make detailed comparisons difficult.

Transport values for the IF inflow have also been estimated by ocean models and Sandø et al. (2012) found an average inflow of 4.7 ± 1.2 Sv using a high-resolution model. The flow over the complicated topography of the IFR remains challenging to model, however, and Olsen et al. (2015) have argued that feedback mechanisms between the IF inflow and the IF overflow make it difficult to disentangle the IF inflow from the net flow across the IFR (IF inflow minus IF overflow).

4.2 The Faroe Current in a climate perspective

The inflow of Atlantic water to the Nordic Seas plays two main roles in the climate system: (1) it transports heat into the Arctic Mediterranean, which affects sea ice and marine conditions, as well as the climate of the surrounding land masses, and (2) it transports salt into the region, which is a precondition for the thermohaline ventilation and hence the circulation system both locally and more globally through the North Atlantic THC.

In the literature, the Atlantic inflow is traditionally split into three separate branches (e.g., Østerhus et al., 2005). Based on similar observational period and methodology as ours, average transport values have been reported for the branch west of Iceland (the North Icelandic Irminger Current) by Jónsson and Valdimarsson (2012) and for the flow through the Faroe–Shetland Channel by Berx et al. (2013). When these values are compared with our results (Table 4), the Faroe Current is found to carry more than 50 % of the total volume transport and 48 % of the total heat transport relative to 0 °C.

This comparison does not take into account the flow of Atlantic water over the shelf region between the Faroe–Shetland Channel and the European continent through various passages including the English Channel. We have no reliable estimate of the combined transports associated with this flow, but the scant observational evidence (Turrell et al., 1990; Childers et al., 2014; Prandle, 1996) indicates that it is well below 1 Sv.

When considering the whole Arctic Mediterranean, we also need to include the inflow through the Bering Strait, where the volume transport increased from 0.7 to 1.1 Sv between 2001 and 2011. The temperature of the Bering Strait

Table 4. Average volume and heat (relative to 0 °C) transport in the three Atlantic inflow branches based on long-term in situ observations.

Inflow branch	Period	Vol. transp.	Heat transp.	Reference
West of Iceland	1994–2010	0.9 ± 0.1 Sv	24 ± 4 TW	Jónsson and Valdimarsson (2012)
Faroe Current	1995–2009	3.8 ± 0.5 Sv	123 ± 15 TW	This study
Faroe–Shetland Channel	1995–2009	2.7 ± 0.5 Sv	107 ± 21 TW	Berx et al. (2013)

inflow is low, however, and its heat transport does not exceed 20 TW (Woodgate et al., 2012).

The Faroe Current thus remains the dominant inflow branch to the Arctic Mediterranean and its heat transport is likely more than one third of the total oceanic heat import to the area. Our observation of an 18 % increase during the 2 decades of observation therefore represents a significant increase in the total oceanic heat import. The two other branches in Table 4 have also experienced increasing temperatures since the mid-1990s (Jónsson and Valdimarsson, 2012; Berx et al., 2013) and it seems likely that their heat transports have increased as well, although the high variability of the transports of these branches makes statistically significant trends difficult to identify.

A discussion on the consequences of increased heat transport is not within the scope of this paper, but we note that oceanic heat transport has been linked to sea ice reduction in the Barents Sea (Årthun et al., 2012) and north of Svalbard (Onarheim et al., 2014) farther downstream on the path of the Atlantic inflow. In the Arctic Ocean, the submerged Atlantic water is partly isolated from the surface by the halocline, but Rippeth et al. (2015) have demonstrated enhanced vertical mixing over steep topography, allowing more heat from the Atlantic layer to reach the surface. On its way northwards, the heat carried by the Atlantic inflow also tends to warm the ambient waters (Skagseth and Mork, 2012; Mork et al., 2014) and enable pelagic fish species to use a larger part of the Norwegian Sea during the feeding period with huge economical perspectives (Utne et al., 2012).

The increased heat transport of the Faroe Current stems partly from the increased temperature of the Atlantic water (Fig. 7) and partly from the increased volume transport (Fig. 8b). The temperature increase mainly occurred from the mid-1990s to 2003, which has been ascribed to a weakening of the subpolar gyre (Häkkinen and Rhines, 2004). As indicated by the inverted gyre index in Fig. 7, the subpolar gyre weakened during this period, which allowed warmer and more saline water from more southern areas west of and over the European continental slope to contribute more intensively to the Atlantic inflow (Hátún et al., 2005). Later variations in the Atlantic water temperature seem more affected by regional air–sea interaction (Larsen et al., 2012).

The increased volume transport is notable in view of the projected decline of the Atlantic meridional overturning circulation (Collins et al., 2013), which is fed by two North Atlantic THC sources, a western (Labrador Sea) and an eastern (Arctic Mediterranean) source (Hansen et al., 2004). It has been suggested that the changes observed in the western North Atlantic may indicate a weakening in that THC source (Robson et al., 2014; Rahmstorf et al., 2015). The main branches of the eastern THC component (Nordic Seas – Arctic Ocean) have been monitored since the mid-1990s, but there we find no convincing evidence for a weakening.

The deep branch of the eastern THC component is dominated by the two main overflows: through the Denmark Strait and through the Faroe Bank Channel. In the Denmark Strait, Jochumsen et al. (2012, 2015) report no significant overall trend and in the Faroe Bank Channel (Hansen and Østerhus, 2007, updated with unpublished data), there has been a slightly increasing trend from 1996 to 2014, although not statistically significant.

The picture is very similar for the upper branch. The inflow branch through the Faroe–Shetland Channel does not show any significant trend (Berx et al., 2013). For the inflow west of Iceland, there are indications of an increasing trend (Jónsson and Valdimarsson, 2012) and Fig. 8b indicates the same for the Faroe Current. It remains to be seen whether these trends will persist.

In this regard, the salt transport is of interest because it may act as a positive feedback on the circulation (Stommel, 1961; Latif et al., 2000). In Table 4, we have not included salt transports; mainly because their values depend critically on the rather ad hoc choice of reference salinity. Regardless of this choice, the salt transport of the Faroe Current has experienced a highly significant increasing trend (Table 3). With reference to the average salinity (34.93) of the Faroe Bank Channel overflow (Hansen and Østerhus, 2007), the salt transport more than doubled from 1993 to 2013 (Fig. 10).

The sensitivity of the THC to freshwater anomalies has been widely studied in modeling experiments, but Glessmer et al. (2014) have recently shown that freshwater anomalies in the Nordic seas are mainly of Atlantic, rather than Arctic, origin. This highlights the importance of the salt transport by the Atlantic inflow and the large increase that we have observed in the Faroe Current should act to stimulate the overflows and thereby also the Faroe Current itself (Hansen et al., 2010). Whether this has played any role in the observed strengthening of the Faroe Current (Fig. 8b) remains to be seen.

Although our time series are long compared to many other transport series, they are still within the timescales of natural variations. Thus, it should be emphasized that the trends

observed may well be caused by natural processes in the climate system.

5 Conclusions

The method used in this study, combining altimetry and in situ observations, has weaknesses, but is found to give more reliable transport estimates than the previously used method based solely on in situ data. This also allows transport estimates for the whole altimetry period, from 1 January 1993, including periods with no in situ current measurements.

Average values for volume and heat (relative to 0 °C) transports of Atlantic water in the Faroe Current were found to be 3.8 ± 0.5 Sv and 124 ± 15 TW, respectively. The average salt transport depends on the choice of reference salinity. All the transports had a seasonal variation with maximum between October and January, although the seasonal amplitudes were only ~ 10 % of the averages and not very persistent. All the transports also increased during the 1993–2013 period. From the trend analysis, percentage (relative to the beginning) annual increases were $0.4 \pm 0.4\,\%\,\mathrm{yr}^{-1}$ for the volume transport and $0.9 \pm 0.4\,\%\,\mathrm{yr}^{-1}$ for heat transport relative to 0 °C. For the absolute salt transport (relative to salinity 0), the annual increase was $2.2 \pm 0.8\,\%\,\mathrm{yr}^{-1}$, whereas the salt transport relative to 34.93 increased by $6 \pm 1\,\%\,\mathrm{yr}^{-1}$.

The Supplement related to this article is available online at doi:10.5194/os-11-743-2015-supplement.

Acknowledgements. The authors wish to thank captains and crew on the R/V *Magnus Heinason* for unfailing support during measurements at sea. Funding for the in situ measurements has been obtained from the Environmental Research Programme of the Nordic Council of Ministers (NMR) 1993–1998, from national Nordic research councils, from the Danish DANCEA programme, and from the European Framework Programs, lately under grant agreement no. GA212643 (THOR) and under grant agreement no. 308299 (NACLIM). Analysis and preparation of this manuscript was mainly funded by the NACLIM project and by the Danish Strategic Research Program through the NAACOS project.

Edited by: M. Hoppema

References

Årthun, M., Eldevik, T., Smedsrud, L. H., Skagseth, Ø., and Ingvaldsen, R. B.: Quantifying the influence of Atlantic heat on Barents Sea ice variability and retreat, J. Climate, 25, 4736–4743, doi:10.1175/JCLI-D-11-00466.1, 2012.

Berx, B., Hansen, B., Østerhus, S., Larsen, K. M., Sherwin, T., and Jochumsen, K.: Combining in situ measurements and altimetry to estimate volume, heat and salt transport variability through the Faroe–Shetland Channel, Ocean Sci., 9, 639–654, doi:10.5194/os-9-639-2013, 2013.

Childers, K. H., Flagg, C. N., and Rossby, T.: Direct velocity observations of volume flux between Iceland and the Shetland Islands, J. Geophys. Res.-Oceans, 119, 5934–5944, doi:10.1002/2014JC009946, 2014.

Collins, M., Knutti, R., Arblaster, J., Dufresne, J.-L., Fichefet, T., Friedlingstein, P., Gao, X., Gutowski, W. J., Johns, T., Krinner, G., Shongwe, N., Tebaldi, C., Weaver, A. J., and Wehner, M.: Long-term climate change: projections, commitments and irreversibility, Chap. 12, in: Climate Change 2013: the Physical Science Basis. Contribution of Working Group I to the Fifth Assessment Report of the Intergovernmental Panel on Climate Change, edited by: Stocker, T. F., Qin, D., Plattner, G.-K., Tignor, M., Allen, S. K., Boschung, J., Nauels, A., Xia, Y., Bex, V., and Midgley, P. M., Cambridge University Press, Cambridge, UK, New York, NY, USA, 2013.

Glessmer, M. S., Eldevik, T., Våge, K., Nilsen, J. E. O., and Behrens, E.: Atlantic origin of observed and modelled freshwater anomalies in the Nordic Seas, Nat. Geosci., 7, 801–805, doi:10.1038/NGEO2259, 2014.

Hansen, B. and Østerhus, S.: Faroe Bank Channel overflow 1995–2005, Prog. Oceanogr., 75, 817–856, doi:10.1016/j.pocean.2007.09.004, 2007.

Hansen, B., Østerhus, S., Hátún, H., Kristiansen, R., and Larsen, K. M. H.: The Iceland–Faroe inflow of Atlantic water to the Nordic Seas, Prog. Oceanogr., 59, 443–474, doi:10.1016/j.pocean.2003.10.003, 2003.

Hansen, B., Østerhus, S., Quadfasel, D., and Turrell, W.: Already the day after tomorrow?, Science, 305, 953–954, 2004.

Hansen, B., Østerhus, S., Turrell, W. R., Jónsson, S., Valdimarsson, H., Hátún, H., and Olsen, S. M.: The inflow of Atlantic water, heat, and salt to the Nordic Seas across the Greenland–Scotland Ridge, Chap. 1, in: Arctic-Subarctic Ocean Fluxes: Defining the Role of the Northern Seas in Climate, edited by: Dickson, R. R., Meincke, J., and Rhines, P., Springer Science + Business Media B. V., 15–43, 2008.

Hansen, B., Hátún, H., Kristiansen, R., Olsen, S. M., and Østerhus, S.: Stability and forcing of the Iceland-Faroe inflow of water, heat, and salt to the Arctic, Ocean Sci., 6, 1013–1026, doi:10.5194/os-6-1013-2010, 2010.

Hátún, H. and McClimans, T. A.: Monitoring the Faroe Current using altimetry and coastal sea-level data, Cont. Shelf Res., 23, 859–868, doi:10.1016/S0278-4343(03)00059-1, 2003.

Hátún, H., Hansen, B., and Haugan, P.: Using an "inverse dynamic method" to determine temperature and salinity fields from ADCP measurements, J. Atmos. Ocean. Tech., 21, 527–534, 2004.

Hátún, H., Sandø, A. B., Drange, H., Hansen, B., and Valdimarsson, H.: Influence of the Atlantic subpolar gyre on the thermohaline circulation, Science, 309, 1841–1844, 2005.

Häkkinen, S. and Rhines, P. B.: Decline of subpolar North Atlantic circulation during the 1990s, Science, 304, 555–559, 2004.

Jakobsen, P. K., Ribergaard, M. H., Quadfasel, D., Schmith, T., and Hughes, C. W.: Near-surface circulation in the northern North Atlantic as inferred from Lagrangian drifters: variability from the mesoscale to interannual, J. Geophys. Res.-Oceans, 108, 3251, doi:10.1029/2002JC001554, 2003.

Jochumsen, K., Quadfasel, D., Valdimarsson, H., and Jonsson, S.: Variability of the Denmark Strait overflow: moored time se-

ries from 1996–2011, J. Geophys. Res.-Oceans, 117, C12003, doi:10.1029/2012JC008244, 2012.

Jochumsen, K., Köllner, M., Quadfasel, D., Dye, S., Rudels, B., and Valdimarsson, H.: On the origin and propagation of Denmark Strait overflow water anomalies in the Irminger Basin, J. Geophys. Res.-Oceans, 120, 1841–1855, doi:10.1002/2014JC010397, 2015.

Jónsson, S. and Valdimarsson, H.: Water mass transport variability to the North Icelandic shelf, 1994–2010, ICES J. Mar. Sci., 69, 809–815, doi:10.1093/icesjms/fss024, 2012.

Larsen, K. M. H., Hátún, H., Hansen, B., and Kristiansen, R.: Atlantic water in the Faroe area: sources and variability, ICES J. Mar. Sci., 69, 802–808, doi:10.1093/icesjms/fss028, 2012.

Latif, M., Roeckner, E., Mikolajewicz, U., and Voss, R.: Tropical stabilization of the thermohaline circulation in a greenhouse warming simulation, J. Climate, 13, 1809–1813, 2000.

Mork, K. A., Skagseth, Ø., Ivshin, V., Ozhigin, V., Hughes, S. L., and Valdimarsson, H.: Advective and atmospheric forced changes in heat and freshwater content in the Norwegian Sea, 1951–2010, Geophys. Res. Lett., 41, 6221–6228, doi:10.1002/2014GL061038, 2014.

Olsen, S. M., Hansen, B., Østerhus, S., Quadfasel, D., and Valdimarsson, H.: Biased thermohaline exchanges with the arctic across the Iceland-Faroe Ridge in ocean climate models, Ocean Sci. Discuss., 12, 1471–1510, doi:10.5194/osd-12-1471-2015, 2015.

Onarheim, I. H., Smedsrud, L. H., Ingvaldsen, R. B., and Nilsen, F.: Loss of sea ice during winter north of Svalbard, Tellus A, 66, 23933, doi:10.3402/tellusa.v66.23933, 2014.

Orvik, K. A. and Niiler, P.: Major pathways of Atlantic water in the northern North Atlantic and Nordic Seas toward Arctic, Geophys. Res. Lett., 29, 1896, doi:10.1029/2002GL015002, 2002.

Østerhus, S., Turrell, W. R., Jónsson, S., and Hansen, B.: Measured volume, heat, and salt fluxes from the Atlantic to the Arctic Mediterranean, Geophys. Res. Lett., 32, L07603, doi:10.1029/2004GL022188, 2005.

Prandle, D., Ballard, G., Flatt, D., Harrison, A. J., Jones, S. E., Knight, P. J., Loch, S., McManus, J., Player, R., and Tappin, A.: Combining modelling and monitoring to determine fluxes of water, dissolved and particulate metals through the Dover Strait, Cont. Shelf Res., 16, 237–257, 1996.

Rahmstorf, S., Box, J. E., Feulner, G., Mann, M. E., Robinson, A., Rutherford, S., and Schaffernicht, E. J.: Exceptional twentieth-century slowdown in Atlantic Ocean overturning circulation, Nat. Clim. Change, 5, 475–480, doi:10.1038/nclimate2554, 2015.

Rippeth, T. P., Lincoln, B. J., Lenn, Y.-D., Green, J. A. M., Sundfjord, A., and Bacon, S.: Tide-mediated warming of Arctic halocline by Atlantic heat fluxes over rough topography, Nat. Geosci., 8, 191–194, doi:10.1038/NGEO2350, 2015.

Robson, J., Hodson, D., Hawkins, E., and Sutton, R.: Atlantic overturning in decline?, Nat. Geosci., 7, 2–3, 2014.

Rossby, T. and Flagg, C. N.: Direct measurement of volume flux in the Faroe–Shetland Channel and over the Iceland–Faroe Ridge, Geophys. Res. Lett., 39, L07602, doi:10.1029/2012GL051269, 2012.

Rossby, T., Prater, M. D., and Søiland, H.: Pathways of inflow and dispersion of warm waters in the Nordic seas, J. Geophys. Res.-Oceans, 114, C04011, doi:10.1029/2008JC005073, 2009.

Sandø, A. B., Nilsen, J. E. O., Eldevik, T., and Bentsen, M.: Mechanisms for variable North Atlantic-Nordic seas exchanges, J. Geophys. Res.-Oceans, 117, C12006, doi:10.1029/2012JC008177, 2012.

Skagseth, Ø. and Mork, K. A.: Heat content in the Norwegian Sea, 1995–2010, ICES J. Mar. Sci., 69, 826–832, doi:10.1093/icesjms/fss026, 2012.

Stommel, H.: Thermohaline convection with two stable regimes of flow, Tellus, 13, 224–230, 1961.

Turrell, W. R., Henderson, E. W., and Slesser, G.: Residual transport within the fair isle current observed during the Autumn Circulation Experiment (ACE), Cont. Shelf Res., 10, 521–543, 1990.

Utne, K. R., Huse, G., Ottersen, G., Holst, J. C., Zabavnikov, V., Jacobsen, J. A., Oskarsson, G. J., and Nøttestad, L.: Horizontal distribution and overlap of planktivorous fish stocks in the Norwegian Sea during summers 1995–2006, Mar. Biol. Res., 8, 420–441, 2012.

Woodgate, R. A., Weingartner, T. J., and Lindsay, R.: Observed increases in Bering Strait oceanic fluxes from the Pacific to the Arctic from 2001 to 2011 and their impacts on the Arctic Ocean water column, Geophys. Res. Lett., 39, L24603, doi:10.1029/2012GL054092, 2012.